Title: Timescales of Antarctic ice shelf loss via basal crevassing

Authors: Alexander T Bradley^{1,2} (alex.bradley@kcl.ac.uk), Niall B Coffey², Ching-Yao Lai²

Note: This paper is a non-peer reviewed preprint submitted to EarthArXiV. It is currently under review at Nature Climate Change.

¹ Department of Geography, King's College London, UK ² Department of Geophysics, Stanford University, CA, USA

Timescales of Antarctic Ice-Shelf Loss by basal-crevassing

A. T. Bradley 1,2 , C. Y. Lai 2 , N. B. Coffey 2

¹Department of Geography, King's College London, UK

²Department of Geophysics, Stanford University, CA, USA

Corresponding author: Alexander T. Bradley, alex.bradley@kcl.ac.uk

Abstract

Antarctic ice-shelves are vulnerable to collapse in a warming climate. However, when this might happen is largely unknown, propagating significant uncertainty into sea-level-rise projections. To constrain this uncertainty, we use fracture modelling to predict the timescales on which crevasses fully penetrate ice-shelves, and consider how these timescales change 10 under future warming. We find that crevassing timescales are highly sensitive to basal-11 melt-rates, through effects on ice temperature, and ice-shelf strain and thinning rates. 12 High basal-melt-rate ice-shelves have short (10s-100s years) timescales, suggesting vul-13 nerability to crevasse-induced collapse in the coming century, whereas ice-shelves with 14 low basal-melt-rates have extremely long (10,000s years) timescales, suggesting they are presently highly stable. However, these long timescales reduce dramatically with increased 16 basal melting predicted in a warming climate, to 100s years using end-of-century basal-17 melt-rates from medium-to-high emissions scenarios. These results highlight a previously 18 under-appreciated link between ocean warming and ice-shelf collapse, and suggest that 19 future sea-level-rise from Antarctica is more sensitive to ocean warming than previously 20 understood. 21

Introduction

32

35

Ice-shelves—the floating extensions of grounded ice-sheets—apply a restraining force 23 ('buttressing') modulating sea-level-rise contributions from ice-sheets (Fürst et al., 2016; Reese et al., 2018; G. H. Gudmundsson et al., 2019, 2012; G. Gudmundsson, 2013). Ice-25 shelves lose mass in two ways: basal melting and calving (Rignot et al., 2013; Greene et 26 al., 2022; Fricker et al., 2025); though both are natural parts of an ice-shelf's lifespan, 27 increases in both have been implicated in ongoing net ice loss from the Antarctic Ice-28 Sheet (AIS) (Pritchard et al., 2012; Joughin et al., 2021). Increases in basal melting lead 29 to progressive buttressing loss (Reese et al., 2018; G. H. Gudmundsson et al., 2019); calv-30 ing, however, is discrete, resulting in near-instantaneous loss of ice-shelf area (R. Alley 31 et al., 2023; Bassis et al., 2024) and often results in ice velocity increases (Fürst et al., 2016), sometimes dramatically. In extreme cases, ice-shelves may 'collapse', with the entire ice-shelf lost rapidly, e.g. Larsen B Ice-Shelf in 2002 (T. A. Scambos et al., 2000; Rignot et al., 2004; T. Scambos et al., 2013) and the Conger Ice-Shelf in 2022 (Walker et al., 2024).

Basal-crevasses (McGrath et al., 2012; Luckman et al., 2012) – large cracks which form at the base of ice-shelves – are crucial to ice-shelf loss because their through penetration can induce rifts (Lipovsky, 2020; Bassis et al., 2008a) – full-shelf thickness fractures, from which large tabular icebergs form (Joughin & MacAyeal, 2005). Lai et al. (2020) demonstrated that many ice-shelves fringing the AIS are vulnerable to extensive crevasse-induced (basal or surface) loss of area or collapse (Lai et al., 2020), including large swathes that provide significant buttressing (Fürst et al., 2016). Here, we focus on vertically-propagating basal-crevasses because they are theoretically more vulnerable than surface crevasses (Lai et al., 2020) and are likely the more dominant where surface melt is not present in significant quantities. Once vertical crevasses penetrate through the thickness, they form rifts which can propagate horizontally. Rift propagation can lead to tabular iceberg calving. Modeling rift propagation timing and trajectory requires higher-order physics (Bassis et al., 2008b; Lipovsky, 2020; Huth et al., 2023) that may not be well-constrained observationally and is therefore left for future research. Inclusion of rift propagation may further increase the mass loss from ice shelves.

Current ice-shelf loss vulnerability estimates lack an associated timescale: it is not understood when ice-shelf area will be lost. Loss of ice-shelf area typically results in reduced buttressing, and thus ice acceleration and increased sea-level-rise contributions (G. H. Gudmundsson et al., 2019). For example, following its collapse, glaciers feeding the Larsen B Ice-Shelf increased in velocity by 3–7 times (T. A. Scambos et al., 2004). When ice-shelf loss happens is, therefore, a strong control on how much sea-level-rise will occur in the coming centuries. This uncertainty may be up to two orders of magnitude: on one hand, simulations (Edwards et al., 2021; Seroussi et al., 2020; Bett et al., 2024; DeConto et al., 2021; Coulon et al., 2024) with ice-shelves remaining fully intact project a centimer scale Antarctic contribution to sea-level-rise over the next century; on the other, simulations with ice-shelves instantaneously removed (Sun et al., 2020), project metre scale sea-level-rise on the same timescale. To constrain these uncertainties, we consider two questions: firstly, under current conditions, how long might it take for significant loss of ice-shelf area, resulting from basal-crevasses penetrating through ice-shelves, to occur? Secondly, how might these timescales change under future warming?

Results

Ice-shelf crevassing is sensitive to basal melting

We first consider how basal melting affects ice-shelf crevassing, via its impact on internal ice temperatures. Ice temperature exerts a leading order control on ice-shelf crevassing (Lai et al., 2020; Coffey et al., 2023) because ice viscosity is sensitive to temperature (Hooke, 1981), and the magnitude of extensional stresses in ice, which promote crevasse formation, are proportional to the viscosity (methods).

Over the AIS, advection dominates heat transfer over diffusion (supplementary figure 1). In this case, ice-shelves temperatures are approximately (Sergienko et al., 2013) (methods)

$$T(x,\hat{z}) = T_g(\hat{z}) + T_d(x) \exp\left(-\frac{\hat{z}}{\ell}\right), \quad \ell = \frac{\kappa}{\dot{m}H}.$$
 (1)

Here, x is an along flow co-ordinate (figure 1a), $\hat{z}(x) = z/H(x)$ a dimensionless vertical co-ordinate, with z=0 at the ice-shelf base, H=H(x) the ice thickness, κ the ice thermal diffusivity, and \dot{m} the basal-melt-rate. The temperature profile (1) is partitioned into $T_g(\hat{z})$, the depth dependent grounding-line ice temperature, which is advected into the ice-shelf, and $T_d>0$ a boundary term that enforces the basal boundary condition, that the ice is at the local freezing point. There is no complete picture of the thermal structure of Antarctic ice-shelves, but modelling (Wang et al., 2022; Grosfeld & Thyssen, 1994) and borehole observations (Wang et al., 2022; Eicken et al., 1994; Kobs et al., 2014; Tyler et al., 2013) support the equation (1) temperature profile (methods).

Ice temperature (equation (1)) is highest at the base, where melting provides a latent heat flux source into the ice, and transition to the cold surface temperatures across their thickness (figure 1a). This basal warming effect is confined to a region of dimensionless thickness ℓ (equation (1)), which is inversely proportional to the basal-melt-rate. Therefore, ice-shelves with higher basal-melt-rates (lower ℓ) have narrower basal warming regions, and temperatures transition to colder surface temperatures over a shorter distance (figure 1a). Hence, ice-shelves with high basal-melt-rates have theoretically lower depth-average temperatures. Colder ice has higher viscosity (Hooke, 1981), leading to increased extensional stresses (which depend exponentially on ice temperature (Hooke,

1981)) and thus larger basal crevasses. Therefore, all else equal, higher basal-melt-rates promote larger crevasses. This theoretical result is supported by observations indicating a strong correlation between basal-melt-rates and ice-shelf basal roughness – a proxy for basal-crevasse penetration distance – across Antarctica (Watkins et al., 2021, 2024).

97

99

100

101

102

103

104

105

106

107

109

110

111

112

113

114

115

116

117

118

119

120

121

122

123

124

125

126

127

Figure 1b (at time = 0), shows that, all-equal except basal-melt-rates, basal-crevasses penetration as determined by fracture models (linear elastic fracture mechanics, LEFM, methods) is smaller in a column of ice with a low basal-melt-rate than in a column of ice with a high basal-melt-rate. Besides the melting enhanced-crevassing mechanism described here, previous work (Bassis & Ma, 2015) shows that both melting in basal-crevasses and ductile deformation-induced basal-crevasse enlargement can enhance tensile stresses above the crevasse, promoting further brittle crevasse propagation. Although not considered here, this mechanism may further reduce the ice loss timescales reported here.

At t=0, basal-crevasses penetrate a portion of the ice-shelf (36% and 50% of the ice-shelf thickness for the warm and cold cases, respectively). The basal-crevassing timescale, denoted τ , is determined as the time taken for the crevasse to penetrate the entire ice column thickness, when it is thinned under a given (constant) thinning rate (see supplementary figure 8 and methods). For an ice-shelf in tension (positive strain rates), background resistive stress acts to open basal-crevasses, and vice versa when in compression (negative strain rates); assuming that resistive stresses remain constant, thinning of a column of ice promotes enhanced basal-crevasse penetration (methods). This is modulated by a widening of the warm basal region with thinning (increasing ℓ as H reduces, equation (1)), which increases the average ice-shelf temperature, promoting reduced crevasse penetration. For low basal-melt-rates, the temperature profile adjusts significantly during thinning (figure 1a), whereas for high basal-melt-rates, changes in the profile are minor, i.e. the stabilizing effect of increasing ice temperature with thinning is only important for low basal-melt-rates. Not only is the basal-crevasse penetration distance lower for the low basal-melt-rate case before any thinning (figure 1b), but the stabilizing effect of increases in ice temperature with thinning is greater than with a high basal-meltrate. Consequently, the crevassing timescale for a column of ice with a high basal-meltrate may be considerably shorter than for a column with a low basal-melt-rate. In the example shown in figure 1b, the crevassing timescale is 80% longer in the low basal-meltrate case, under otherwise identical conditions. For other basal-melt-rates and initial ice

thicknesses (the thickness of the column prior to thinning), the crevassing timescale may be enhanced by as much as 500%, compared to a very high basal-melt-rate case (figure 1c).

As well as ice temperature, basal-melt-rates also influence both ice-shelf strain rates and thinning rates, which feed back on crevasse penetration distances. Crevasse penetration distances are highly sensitive to strain rates (Lai et al., 2020), because resistive stresses in ice increase with strain rates (equation 11). All else equal, higher strain rates result in increased crevasse penetration distances and thus reduced crevasse timescales. Empirically, we find that average strain rates on Antarctic ice-shelves are strongly correlated with average basal-melt-rates (p < 0.001, figure 2a). Observations also indicate that strain rates and basal-melt-rates are highly correlated with ice-shelf basal roughness – a proxy for basal-crevasse depth (Watkins et al., 2024). Although the relation-ship between strain rates and basal-melt-rates is complex, depending on the entire ice-sheet system, a plausible explanation is that higher basal-melt-rates reduce ice-shelf buttressing, increasing ice-sheet flow speeds and thus strain rates.

Additionally, basal-melt-rates are highly correlated with thinning rates (p < 0.001, figure 2b). Increased thinning rates will result in reduced crevasse timescales because columns of ice will sooner reach the thickness that at which a through-thickness crevasse propagates.

In summary, increases in ice-shelf basal-melt-rates not only reduce expected crevassing timescales via changes in ice temperature, but also via increases in both ice-shelf strain and thinning rates. Thus, a strong dependence of crevasse timescales on basal-melt-rates is to be expected in practice.

Circum-Antarctic crevassing- and ice loss- timescales

Figure 3a shows circum-Antarctic crevassing timescales, determined using observations basal-melt-rates (Adusumilli et al., 2020), thinning rates (Smith et al., 2020), thickness (Fretwell et al., 2013), and strain rates derived from a data-constrained flow model (Wearing, 2017) on a 1km grid (methods), alongside oceanic thermal forcing (Adusumilli et al., 2020).

This map indicates that crevassing timescales are highly sensitive to basal-meltrates: areas with high thermal forcing, and thus high basal-melt-rates, generally have much shorter crevassing timescales than those with low thermal forcing. Broadly, crevassing timescales are shortest in the Amundsen and Bellingshausen Sea sectors, where maximum thermal forcing is above 4 $^{\circ}$ C, while in the Weddell and Ross Seas, thermal forcing is low (< 2 $^{\circ}$ C) and crevassing timescales on adjacent ice-shelves are typically very long. Within this picture, however, there is significant local heterogeneity; e.g. crevassing timescales on the Larsen Ice-Shelves, which are exposed to locally elevated thermal forcing, are much shorter than on the neighbouring Ronne Ice-Shelf, despite both being located in the Weddell Sea sector.

158

159

160

161

162

163

164

165

166

168

169

170

171

172

173

174

175

176

177

178

180

181

182

183

184

185

186

187

188

189

To go beyond these qualitative comparisons, we determine, for each ice-shelf, a 'ice-loss timescale'—the mean of a kernel density estimate of crevassing timescales across the ice-shelf (figure 3b). The ice-loss timescale is interpreted as the timescale on which these ice-shelves will persist. In particular, it should not be interpreted as a prediction of when ice-shelves will collapse (for which a more detailed model is required, see 'Discussion'), but rather represents the timescale on which ice-shelf loss is expected.

ice-loss timescales are strongly dependent on basal-melt-rates (the left-right colour gradient in figure 3b follows red to blue, see also supplementary figure 2). High basalmelt-rate ice-shelves (red in figure 2 and figure 3b), particularly those in the Amundsen Sea sector, have the lowest ice-loss timescales. Most Amundsen Sea sector ice-shelves have ice-loss timescales of O(10s years). This suggests that may already been preconditioned for significant ice loss in the coming decades, supporting similar suggestions based on observations from Pine Island Glacier (Lhermitte et al., 2020) and Thwaites Glacier (Pettit et al., 2021). The rapidly retreating Thwaites Glacier has the lowest ice-loss timescale of those ice-shelves considered, but this should be taken with caution owing to the sparsity of data available for this ice-shelf. Although the buttressing provided by these iceshelves varies—for example, the Pine Island Ice-Shelf provides strong buttressing (Bradley, De Rydt, et al., 2022), whereas the Thwaites Ice-Shelf provides limited buttressing (G. H. Gudmundsson et al., 2023)—models unanimously agree that losing ice-shelves in the Amundsen Sea sector will result in elevated sea-level-rise (Sun et al., 2020). Thus, our results support evidence that substantial sea-level-rise from the West Antarctic ice-sheet before the end of the century may be already committed (Bett et al., 2024; van den Akker et al., 2024).

At the other end of the spectrum, low basal-melt-rate ice-shelves including the Amery, Ronne, Ross, and Filchner have ice-loss timescales of O(1000s years). This suggests that,

under current conditions, these ice-shelves are highly stable and will continue to buttress their large inland sectors, limiting associated sea-level-rise contributions. It should be noted, however, that under high emissions scenarios, some ice streams feeding these ice-shelves undergo significant retreat even without substantial ice-shelf loss (Seroussi et al., 2023).

190

191

192

193

194

195

196

197

198

202

203

204

205

206

207

208

209

210

212

213

214

215

216

217

218

Outliers to this picture are the Totten and Moscow University ice-shelves, which, despite very high basal-melt-rates (figure 2a), have long ice-loss timescales (figure 3b). This is because these ice-shelves are relatively thick (supplementary figure 3d) and, despite high basal-melt-rates, experience relatively low thinning rates (figure 2b). Additionally, the Brunt ice-shelf displays anomalously short collapse times, resulting from relatively high strain (figure 2a) and thinning (figure 2b) rates. A short ice-loss timescale for Brunt is consistent with significant calving which took place in January 2023 (Marsh et al., 2024).

We compare ice-loss timescales obtained using three crevasse-depth models: LEFM (Van der Veen, 1998; Jiménez & Duddu, 2018; Lai et al., 2020), the zero-stress approximation (Nye, 1955; Jezek, 1984; Benn et al., 2007; Nick et al., 2010) and the horizontal force balance (HFB) theory (Coffey et al., 2023; Buck, 2023). LEFM models tend to overestimate crevasse depths compared with HFB and the zero-stress approximation (Coffey et al., 2023), and thus underestimate crevasse timescales, due to the assumed stress concentration at the crack tip, which may not exist due to ocean melting and freezing. ice-loss timescales using these theories are obtained using the procedure outlined above, but with crevasse depths at each timestep calculated using the relevant theory (methods). We find that, regardless of the crevasse depth theory used, the ice-loss timescale remains on the same order of magnitude, with strong dependence on the basal-melt-rate (figure 3b), supporting our conclusions. The ice-loss timescale computed using the zero-stress theory are consistently larger than those obtained using LEFM, in agreement with the rifting stress predictions of Coffey et al. (2023). This suggests that the use of HFB or LEFM crevasse-depth models in ice-sheet models may yield larger future ice-shelf loss and thus sea-level-rise contributions than previously predicted with the zero-stress theory (Sun et al., 2017).

ice-loss timescales under future warming

219

221

222

223

224

225

226

227

229

230

231

232

233

234

235

236

237

238

239

240

241

242

244

245

246

247

248

249

250

The ice-loss timescales reported above are appropriate in the case that basal-meltrates, strain rates, and thinning rates remain at their present day values. In practice, however, these will respond to climatic changes resulting from increasing anthropogenic emissions. To assess the sensitivity of ice-loss timescales to future warming, we repeat the simulation presented in figure 3 a, but with a uniform increases in melting, $\Delta \dot{m}$, applied to each ice-shelf. To account for the concomitant increase in strain and thinning rates (figure 2), we simultaneously increase these quantities in line with best fits to the empirical relationship between them (i.e. according to the black dashed lines in figure 2, methods).

We find that ice-loss timescales respond strongly to increases in basal-melt-rate (figure 4a; note that the ordinate axis is logarithmic). For example, a uniform 1 m year⁻¹ increase in basal-melt-rate leads to a >50% reduction in the ice-loss timescale for all ice-shelves whose ice-loss timescales under present conditions is above 100 years (figure 4a). A uniform 10 m year⁻¹ increase in basal-melt-rate results in a reduction in the ice-loss timescale of every ice-shelf by at least an order of magnitude.

To place these results in a realistic context, we use output from a coupled atmosphereocean-ice-sheet model (Park et al., 2023) to determine plausible future increases in basalmelt-rates (supplementary figure 7, using the ensemble mean at the year 2100) and compute associated ice-loss timescales (methods). The results (figure 4b-e) indicate that iceloss timescales associated with end-of-century basal-melt-rates are highly sensitive to the emission pathway. For the Ross Ice-Shelf, ice-loss timescales remain on the order of millennia under SSP1-1.9, but reduce dramatically to decadal-to-centennial timescales under SSP2-4.5 and SSP5-8.5. Under the low warming SSP1-1.9 scenario, Filchner Ice-Shelf basal-melt-rates are lower at the end of the century (consistent with (Nicholls, 1997; Naughten et al., 2021)) and collapse times therefore increase. However, under more extreme scenarios, Filchner Ice-Shelf ice-loss timescale similarly reduce sharply. ice-loss timescales for the Ronne and Amery ice-shelves are both reduced by a factor of approximately onethird under SSP1-1.9, with ice-loss timescales under SSP5-8.5 an order of magnitude smaller than present day values. These results suggest that, while ice-shelves with low basal-meltrates appear to be highly stable at present, future warming may dramatically alter their stability. Changes in crevasse timescales are strongly dependent on the emissions pathway taken, even without considering surface processes such as hydrofracture (Weertman, 1974; T. Scambos et al., 2009), which are expected to become more common under future warming (Gilbert & Kittel, 2021; K. Alley et al., 2018; Banwell et al., 2013; DeConto & Pollard, 2016; Lai et al., 2020). However, this increased risk may be offset by the increase in ice temperature associated with an increase in surface air temperatures. Future work should aim to disentangle these processes.

Discussion

There are three key results of our study: firstly, ice-shelves with high basal-melt-rates, particularly Thwaites, Pine Island, and Larsen C, have ice-loss timescales of 10s-100s of years, supporting suggestions that they are preconditioned to collapse, or lose significant ice-shelf area, before the end of the century, and thus their upstream catchments may already have committed sea-level-rise; secondly, low basal-melt-rate ice-shelves, particularly Ross, Ronne, and Filchner which buttress large swathes of the AIS, are highly stable in their present configurations, limiting their sea-level-rise potential; finally, ice-loss timescales are very sensitive to future increases in basal-melt-rate, with most ice-shelves potentially preconditioned to collapse by 2100 under extreme forcing scenarios. The response of these timescales depends heavily on emissions, highlighting the urgency of reductions to promote the longevity of Antarctic ice-shelves and thereby limit sea-level-rise.

More generally, we have reinforced that crevassing is highly dependent on basalmelt-rates: crevassing and melting are not independent mechanisms driving mass loss
from ice-shelves, but are strongly coupled. This provides a mechanistic understanding
which supports observational evidence in Antarctica (Y. Liu et al., 2015) and Greenland (Luckman
et al., 2015) linking increases in basal-melt-rates with increases in ice-shelf calving.

We stress that our ice-loss timescales are not predictions of when ice-shelves are predicted to collapse, but rather a timescale associated with their persistence. Determining exactly when ice-shelves might calve or collapse requires the use of an ice-sheet model with a calving law (Wilner et al., 2023), since removal of sections of the ice-shelf will feed back on ice-shelf flow, via reduced buttressing. Reduced buttressing will result in increased strain and thinning rates, so this feedback may reduce our ice-loss timescales further. Loss of ice-shelf area can also increase basal-melt-rates (Bradley, Bett, et al., 2022), poten-

tially reducing ice-loss timescales. High basal-melt-rates can also result lead to formation of weak zones which serve as nucleation points for rifting and calving (Watkins et al., 2024). On the timescales reported here, grounding-lines—where the ice transitions from grounded to floating—of ice-sheets may change; where grounding-lines retreat, new sections of ice-shelf are exposed, potentially providing additional buttressing, increasing ice-loss timescales.

282

283

284

285

286

287

288

289

290

291

294

295

296

297

298

299

300

301

303

304

305

306

307

308

309

310

311

312

313

314

We have made several simplifying assumptions, which should be noted. We assume uniform basal temperature, surface temperature, and geothermal heat flux in the temperature profile (methods). In practice, the geothermal heat flux is spatially heterogenous, and, in particular, elevated around West Antarctica (Fisher et al., 2015); this would result in warmer ice, with concomitant reduced crevasse depths and enhanced ice-loss timescales. In addition, the temperature profile (equation (1)) does not account for isothermal marine ice, which is prevalent on some ice-shelves (Craven et al., 2009; Wang et al., 2022). Including this would increase the average temperature, reducing crevasse propagation. The LEFM theory assumes that ice columns evolve independently of their neighbours, and that narrow crevasses (below the 1km grid resolution) may be parameterized like this. In reality, crevasse propagation through the entire thickness of an ice-shelf can alter the surrounding stress field, potentially triggering further crevassing (Banwell et al., 2013; Robel & Banwell, 2019). Interacting crevasses can reduce the stress at crevasse tips, reducing propagation. However, the HFB theory can be considered an end member in which crevasses occurring in sets, and shows similar ice-loss timescales, suggesting the effect of interacting crevasses does not play a leading order role. We have assumed that large-scale basal-melt-rates are appropriate within localised crevasses, though practically there may be local heterogeneity (Schmidt et al., 2023).

We have considered only basal-crevasses, and assumed that sufficient initial flaws of size O(10) meters are present to initiate crevasses (Coffey et al., 2023). Basal-crevasses are usually larger than surface-crevasses due to the water pressure within them; including surface crevasses, which may grow and join basal-crevasses, may reduce ice-loss timescales. Surface crevasses are vulnerable to hydrofracture, which might promote rapid ice-shelf disintegration (Banwell et al., 2013; Robel & Banwell, 2019). The presence of both basal and surface crevasses may, however, suppress their mutual propagation, owing to the moments they generate (Zarrinderakht et al., 2023), as can ocean restoring forces (Buck & Lai, 2021; Zarrinderakht et al., 2022). Other in-crevasse melting and freezing not included

here, could also alter crevassing stability: low basal-melt-rates can cause accretion of marine ice filling crevasses, while high basal-melt-rates can cause vigorous melting within crevasses and lead to further brittle failure (Bassis & Ma, 2015). In ductile modes, basal refreezing can suppress crevasse propagation; for low basal-melt-rate ice-shelves, where refreezing is likely, this may enhance crevassing timescales. We took a pessimistic estimate of recent thinning rates (methods); while this may affect absolute values of ice-loss timescales, it shouldn't affect their magnitudes, nor the differences in scales between high and low basal-melt-rate ice-shelves. We assume strain rates remain constant during thinning, whereas in practice, strain rates could reduce; however, we find that, for plausible changes in strain rates, the order of the magnitude of our timescale results are not affected (methods).

As the ocean warms, ice-shelves are expected to experience increased basal melting, directly contributing to their mass loss. Here, we have shown that elevated basalmelt-rates on ice-shelves can substantially reduce timescales of ice-shelf loss via basal crevassing through reductions in mean temperature, and increases in thinning rates and strain rates. Our circum-Antarctic map of ice-loss timescales demonstrates this sensitive dependence. These timescales are dramatically reduced by 2100 under moderate to high emissions scenarios. Our results stress the need for urgent emissions reductions to preserve Antarctic ice-shelves and thus prevent significant sea-level-rise contributions from the AIS.

Data Availability

Code to perform simulations and produce the figures contained in this paper is held in an open GitHub repository: https://github.com/alextbradley/Collapse-Timescale.

Acknowledgements

A. T. B. is supported by the NERC Grant NE/S010475/1 and the PROTECT project, which received funding from the European Union's Horizon 2020 research and innovation program under grant agreement no. 869304. C.-Y.L. acknowledges partial support from NSF's Office of Polar Programs through OPP-2344690.

Methods

345

346

351

352

355

356

357

358

359

360

361

362

Ice-shelf temperature profiles

In an ice-shelf, viscous heating is expected to be small and thus the internal ice temperature T approximately satisfies the advection-diffusion equation

$$\frac{\mathrm{D}T}{\mathrm{D}t} = \nabla \cdot (\kappa \nabla T) \tag{2}$$

where t represents time, κ is the thermal diffusivity of ice, and ∇ the differential operator with respect to a co-ordinate system (x, y, z), where we take z to denote the vertical co-ordinate. Assuming that the ice has a spatially constant thermal diffusivity and a steady ice temperature, (2) reduces to

$$\nabla \cdot (\mathbf{u}T) = \kappa \frac{\partial^2 T}{\partial z^2}.$$
 (3)

Here, \mathbf{u} is the ice velocity and we have suppressed the T_{xx} and T_{yy} terms on the right-hand-side because they are small by comparison with T_{zz} since ice-sheets have high aspect ratios. Taking x to be everywhere locally parallel to the flow and y everywhere local perpendicular to the flow (so that the y component of velocity is identically zero), and invoking incompressibility of the flow, equation (3) reduces to

$$u\frac{\partial T}{\partial x} + w\frac{\partial T}{\partial z} = \kappa \frac{\partial^2 T}{\partial z^2} \tag{4}$$

where u and w components of velocity in the x and z directions, respectively.

Equation (4) was considered by Sergienko et al. (2013). They show that for a large Peclet number, $\text{Pe} = H^2 |\mathbf{u}|/(L\kappa) \gg 1$, where H is the ice thickness, and L the length-scale of the flow, the solution to (4) on floating ice-shelves may be expressed as

$$T(x,\hat{z}) = T_g \left[\xi(x,\hat{z}) \right] + \left\{ T^*(x) - T_g \left[\xi(x,0) \right] \right\} \exp\left(-\frac{\hat{z}}{\ell} \right)$$
 (5)

where $\hat{z} = z/H$ is a dimensionless vertical co-ordinate with origin at the ice-shelf base and measured upwards, with H = H(x) the local ice thickness, $\ell = \kappa/(\dot{m}H)$ is the lengthscale of the boundary warming effect, with \dot{m} the local melt rate, $T^*(x)$ is the local freezing temperature, T_g is the depth-dependent temperature profile at the groundingline (where x = 0), and

$$\xi(x,\hat{z}) = 1 - \frac{1-\hat{z}}{q_a}q(x),$$
 (6)

where q(x) = u(x)H(x) is the ice flux, and q_g is the ice flux at the grounding-line. The solution (5) results from assuming that surface accumulation is negligible, but Sergienko et al. (2013) show that this assumption only makes a small difference to the temperature profile. Note that in the case of a negative basal-melt-rate (i.e. basal freezing) the temperature profile (5) predicts a temperature which grows exponentially away from the ice-ocean interface, which is unphysical. To avoid this scenario, negative basal-melt-rates observed in practice are set to a small positive value (see 'Antarctic ice-loss timescales' below).

Determining the grounding-line temperature is difficult because it depends on the history of ice advected from upstream, and no analytic solution exists. To mitigate this, we follow Sergienko et al. (2013), and take an analytical ice divide temperature profile (Robin, 1955) as the temperature profile at the grounding-line, setting

$$T_g(\hat{z}) = T_s - \frac{Q}{K} \sqrt{\frac{2H_g\kappa}{\dot{A}}} \left[\operatorname{erf}\left(\sqrt{\frac{\dot{A}H_g}{2\kappa}}\right) - \operatorname{erf}\left(\sqrt{\frac{\dot{A}\hat{z}^2H_g}{2\kappa}}\right) \right]. \tag{7}$$

Here T_s is the surface temperature, Q is the geothermal heat flux per unit area, K is the thermal conductivity of ice, H_g is the ice thickness at the grounding-line, \dot{A} is the surface accumulation, and $\operatorname{erf}(\phi) = \int_0^{\phi} \exp(-\lambda^2) \, \mathrm{d}\lambda$ is the error function. The temperature profile (7) is based on a balance between diffusion through the ice column, which is geothermally heated at its base, and cold surface temperatures.

The temperature profile (5) requires the ice flux to be known everywhere along a flowline. This is problematic because, without a coupling to an ice-sheet model, we cannot determine the velocity response to thinning. To alleviate this, we make an 'unconfined ice-shelf' approximation, setting the local ice flux equal to the grounding-line flux. In this case, $\xi = \hat{z}$ and the temperature profile (5) reduces to

$$T(x,\hat{z}) = T_g(\hat{z}) + \{T^*(x) - T_g(\hat{z})\} \exp\left(-\frac{\hat{z}}{\ell}\right).$$
 (8)

In supplementary figure 5, we show a comparison between the temperature profile (5) and the approximation (8) along flowlines taken on the Ross (low basal-melt-rate) and Pine Island (high basal-melt-rate) ice-shelves. In this case, the grounding-line flux

and ice thickness are determined from observations of ice thickness and velocity (see 'Antarctic ice-loss timescales' below). The approximation (8) captures the key features of (5) with relatively small errors (supplementary figure 5e-f), justifying our unconfined iceshelf approximation. The decoupling from the ice flux within the shelf can be seen in particular for the low basal-melt-rate profile (figure 5a), for which the temperature is more clearly advected downstream. Our approximation has the benefit that it does not require the velocity to be defined everywhere in the ice-shelf, but only at the grounding-line. This allows us to extend temperature profiles to areas with missing velocity data, such as at ice fronts (compare figure 5b and d, for example). In general, on ice-shelves with low basalmelt-rates, the approximation (8) overestimates ice temperatures in some regions and underestimates in others, compared to (5) (figure 5e). For ice-shelves with high basalmelt-rates, the approximation (8) systematically overestimates temperatures (figure 5f). This is because, with a higher basal-melt-rate, the flux reduces downstream more quickly (owing to stronger reductions in ice thickness); in this case, $q(x)/q_g$ reduces downstream, so ξ increases (as it does in practice) and the surface, where $\xi = 1$, has a great contribution, rendering temperatures colder.

Determining the crevassing timescales

390

391

392

393

394

395

397

400

401

402

403

404

405

407

410

411

412

413

414

415

416

417

418

419

420

421

Crevassing timescales are determined by considering how long from now, under current conditions, it will take for a crevasse to penetrate through the thickness of a fixed grid cell (corresponding to a column of ice). For a column of ice (see supplementary figure 8) with a given thickness, we first use the basal melt rate to determine the ice shelf temperature profile, as outlined in "Ice-shelf temperature profiles". We then compute the penetration distance d of a basal crevasse using three distinct crevasse-depth models, the linear elastic fracture mechanics framework outlined in "Linear elastic fracture mechanics theory", the horizontal force balance (HFB) model, and the zero stress approximation, assimilating observations of ice shelf strain rates. If this penetration distance is equal to the ice thickness, the crevasse timescale for this particular grid point is said to be zero; otherwise, the ice thickness is time stepped to determine the crevasse timescale (see below).

The crevasse depth in the column of ice at time $t = \delta t$ is time stepped by reducing the ice thickness H in the column to $H \to H + \mathrm{d}H/\mathrm{d}t \times \delta t$, where $\mathrm{d}H/\mathrm{d}t$ is the ice shelf thinning rate, and the crevasse penetration distance is then determined based on

the instantaneous ice thickness following the procedure outlined in the previous paragraph (supplementary figure 8). The basal melt rate and strain rate are assumed to remain constant during this step. This procedure is repeated for $t = 2\delta t, 3\delta t, \dots, n\delta t$, where $n\delta t$ is the first time at which the crevasse penetrates through the entire ice thickness.

422

423

424

425

426

427

428

429

430

431

432

433

435

436

437

438

439

440

441

442

443

444

445

446

448

449

450

451

452

453

If the thinning rate is positive (i.e. the column of ice is getting thinner with time), the dimensionless crevasse depth d/H (see supplementary figure 8)— the ratio of the crevasse penetration distance to the ice thickness — necessarily increases in time and the crevassing timescale is not defined. If the thinning rate is negative, dimensionless crevasse depths decrease in time, and the situation is more complicated: if the dimensionless crevasse depth is one prior to any thinning, the crevassing timescale is set to be 0, otherwise, the crevassing timescale is not defined.

In the results shown here, ice thickness updates have a timestep of $\delta t=1$ year, which effectively sets the temporal resolution of the results.

The crevassing timescale is also not defined in regions with negative strain rates because fracture models necessarily predict zero crevasse depth (see 'Linear elastic fracture mechanics theory' below).

In all results shown here, we assume a constant basal temperature of -2 °C. In practice, ice-shelf basal temperatures are necessarily at the local freezing temperature, which depends on the local salinity and depth. Determining this in detail requires the use of a coupled-ice ocean model and is beyond the scope of this work. However, the depthand salinity-dependence on basal-temperatures are fairly weak, justifying our use of a constant value. This constant value agrees well with observations from the Amery iceshelf (supplementary figure 4). To isolate the effects of basal melting on temperature profiles, we assume a constant surface temperature $T_s = -22$ °C, a constant geothermal heat flux $Q = 48 \text{ W/m}^2$, and accumulation rate $\dot{A} = 0.1 \text{ m a}^{-1}$. We assume a constant ice fracture toughness $K_{Ic} = 150 \text{ kPa m}^{1/2}$; in general the ice fracture toughness may be temperature dependent, though this relationship is not well understood, and laboratory experiments suggest that fracture toughness is only weakly dependent on temperature in the range considered here (H. W. Liu & Miller, 1979), and that for low strain rate processes, a value of 150 kPa m^{1/2} is appropriate (Litwin et al., 2012). We consider non-linear viscous ice rheology, taking a Glen flow law with Glen's flow exponent n =3.

Here, we assume that strain rates remain constant during thinning. However, in practice, strain rates may be expected to reduce during thinning, potentially feeding back on ice loss timescales. In particular, in the case of an unconfined ice-shelf, the stress τ in the ice-shelf is known analytically: $\tau = \rho g'H$, where ρ is the ice density, g' is the reduced gravity, and H is the ice thickness, which is related to the strain rate $\dot{\epsilon}_{xx}$ via $\tau = 2\mu\dot{\epsilon}_{xx}$, with μ the ice viscosity. With a power law viscosity, $\mu \sim 1/\tau^n$, where $n \geq 0$ is a rheological exponent, we find that $\dot{\epsilon}_{xx} \sim H^n$.

To assess the sensitivity of the ice loss timescale to variations in strain rate, we determined the loss timescale for each ice-shelf according to this scaling, i.e. by setting the strain rate at each timestep in the simulation to $\dot{\epsilon} = \dot{\epsilon}_0 (H/H_0)^n$ where $\dot{\epsilon}_0$ and H_0 are the initial strain rate and thickness at this grid point (i.e. those from the data sets), respectively. We do so in two cases: one with n=1 and one with n=3. Supplementary figure 9 shows distributions of crevassing timescales alongside ice loss for n=0 (constant strain rate), n=1 (a linear rheology), and n=2 (a non-linear rheology). We see that, as expected, increasing the exponent increases the ice loss timescale (squares are above triangles, which are above points). However, crucially, the timescales remain on the same order of magnitude, and display the same sensitivity to basal melt rates.

Antarctic ice-loss timescales

To construct the map of circum-Antarctic crevassing timescales, we use observations of basal-melt-rates (Adusumilli et al., 2020), thinning rates (Smith et al., 2020) (supplementary figure 3a), ice thickness (Fretwell et al., 2013) (supplementary figure 3d), strain rates (Wearing, 2017) (supplementary figure 3c) and ice velocity (Gardner et al., 2018). These products have good coverage over Antarctic ice-shelves, with 82% of ice-shelf points in the bathymetry datasat having a well-defined thinning rate, strain rate, and basal-melt-rate. Much of the data gap arises from the basal-melt-rate product, highlighting the need for continued improvement in such products.

Basal-melt-rate data is used to determine the ice temperature profiles, which set the ice viscosity (see 'Linear elastic fracture mechanics theory'). Since the temperature profile (8) is not well-defined for any non-positive basal-melt-rate (see 'Ice-shelf temperature profiles'), we set the basal-melt-rate on all grid points with a negative basal-meltrate to be a small positive value (here 0.1 m year⁻¹, supplementary figure 3f). This adjustment does not have an affect on shelves with high basal-melt-rates (i.e. warm water ice-shelves), but is relevant for low basal-melt-rate ice-shelves. We expect that adjusting the basal-melt-rate in this way would increase the modelled ice temperature (relative to actual), because basal-melt-rate reflects a source of heat into the ice. Thus, modelled ice temperatures on low basal-melt-rate ice-shelves may be warmer than they are in practice, suggesting that crevasse timescales reported here may be longer than they should be on these shelves. When compared with borehole estimates on the Amery Ice-Shelf, (a low basal-melt-rate ice-shelf), modelled temperatures are indeed marginally larger than observed temperatures (supplementary figure 4), but display similar agreement to observations with a full thermomechanically coupled ice-sheet model.

Ice-shelf thinning rates (Smith et al., 2020) are used to determine ice-shelf thickness updates. The pattern of ice-shelf thinning rates (supplementary figure 3a) represents an average over a long period (2003–2019), is highly spatially heterogeneous, and features large errors (Smith et al., 2020) which dominate the signal in places. Additionally, during this period, many ice-shelves have accelerated. To smooth these effects, we use a constant thinning rate on each ice-shelf (supplementary figure 3b). This value is set to equal one standard deviation above the mean thinning rate on each ice-shelf; this is an ad-hoc measure to account (somewhat) for the acceleration of ice-shelf thinning over the long observational period, and permits ice-loss timescales to be constructed because almost every ice-shelf is thinning when measured in this way (according to this measure, all ice-shelves, except for an isolated region in Dronning Maud Land, have a positive thinning rate). By using the standard deviation, we retain the correct order of magnitude of thinning in the calculation of crevasse timescale. The dataset of (Smith et al., 2020) is provided on a 5km grid and downscaled to our 1km grid using linear interpolation.

Linear elastic fracture mechanics theory

A detailed background to linear elastic fracture mechanics applied to ice-shelves is presented in the supplementary information of Lai et al. (2020). Here, we provide a brief overview. In the tensile fracture LEFM framework for basal-crevasses, crevasse depths are determined by considering three stresses: the background resistive stress in the ice-shelf, the water pressure within basal-crevasses, and the weight of the ice (supplementary figure 6). When the ice-shelf is in tension (positive strain rates), background resistive stresses act to open basal-crevasses, while, when in compression (negative strain rates),

background resistive stresses act to close basal-crevasses shut. Above the base of the ice, the water pressure within basal-crevasses is higher than the neighbouring glaciostatic ice pressure, which additionally encourages crevasse propagation. The weight of ice acts to close crevasses, discouraging their propagation. In LEFM, the concentration of stresses near the crevasse tip is expressed as a mode I stress intensity factor K_I , which depends on the stress distribution acting on the fracture surfaces. The material strength of ice is encapsulated though the fracture toughness K_{Ic} (a material property), with fracture propagation possible when $K_I \geq K_{Ic}$. In this linear framework, this stress intensity is expressed as the superposition of terms corresponding to the three components, which vary with the crevasse depth d,

$$K_I = K_I(d) = K_R(d) + K_W(d) - K_L(d).$$
 (9)

The terms on the right-hand side of (9) correspond to tensile resistive stresses, water pressure, and the ice glaciostatic pressure, respectively, and are shown schematically as a function of depth in supplementary figure 6.

To determine the crevasse depth predicted by LEFM, the stress (9) is compared with the fracture toughness of ice. Crevasses may propagate to the depth at which the stress intensity K_I equals the fracture toughness K_{Ic} ; however, these depths only correspond to stable configurations (with respect to stress perturbation) when the stress intensity decreases with increasing crevasse depth (supplementary figure 6): if the stress intensity K_I increases with crevasse depth, it is energetically favourable for the crevasse to grow (supplementary figure 6). The theoretical maximum initial flaw size for basal-crevasses based on LEFM is O(10) meters (Coffey et al., 2023). It is assumed that initial flaws exist in the ice that can grow to stable crack depths in the LEFM framework. Here, we consider only the physically relevant, stable crevasse depths.

The tensile resistive stress term can be expressed as

$$K_R = \int_0^{\frac{d}{H}} \frac{2R_{xx}(\hat{z})}{\sqrt{\pi d}} G\left(\hat{z}, \frac{d}{H}\right) \left[1 - \frac{d}{H}\right]^{-3/2} (1 - \hat{z})^{-1/2} dz$$
 (10)

where H is the ice thickness and G a dimensionless weight function whose analytic form is known (Tada et al., 2000). R_{xx} is the along-flow resistive stress (Van der Veen, 1998, 2013),

$$R_{xx} = 2B(T(z))\dot{\epsilon}_{xx}|\dot{\epsilon}_{xx}|^{1/n-1},$$
 (11)

where B(T(z)) is the ice viscosity, with T(z) the depth-dependent temperature profile, 544 $\dot{\epsilon}_{xx}$ is the along-flow strain rate and n is Glen's flow exponent. The ice viscosity B(T)545 is expressed using a common Arrhenius type relationship fit to lab experiments (Hooke, 546 1981) 547

$$B(T(z)) = B_0 \exp\left[\frac{T}{T_0} - \frac{C}{(T_r - T)^k}\right]$$

$$\tag{12}$$

where $B_0 = 1.928 \times 10^{-5}$ bar $a^{1/3}$, $T_0 = 3155$ K, C = 0.11612 K^{1.17}, and $T_r = 273.39$ K. As the temperature increases, the B(T) decreases, making the resistive stress R_{xx} , and thus the stress intensity component K_R , smaller.

The other terms in (9) are

550

551

555

556

557

558

559

561

$$K_W(d) = \frac{2\rho_w g d^{3/2}}{\sqrt{\pi}} g_b(d)$$
 (13)

$$K_L(d) = \frac{2\rho_i g d^{3/2}}{\sqrt{\pi}} f_b(d) \tag{14}$$

where $\rho_w = 1028.0 \text{ kg m}^{-3}$ and $\rho_i = 918.0 \text{ kg m}^{-3}$ are the densities of seawater and 552 ice, respectively, $g = 9.81 \text{ m s}^{-2}$ is the acceleration due to gravity, and f_b and g_b are di-553 mensionless weight functions 554

$$g_b(d) = \int_0^1 \left(\frac{\rho_i}{\rho_w} \frac{H}{d} - \hat{z}\right) G\left(\hat{z}, \frac{d}{H}\right) \left(1 - \frac{d}{H}\right)^{-3/2} (1 - \hat{z}^2)^{-1/2} d\hat{z}, \tag{15}$$

$$f_b(d) = \int_0^1 \left(\frac{H}{d} - \hat{z}\right) G\left(\hat{z}, \frac{d}{H}\right) \left(1 - \frac{d}{H}\right)^{-3/2} (1 - \hat{z}^2)^{-1/2} d\hat{z}.$$
 (16)

Horizontal force balance and zero stress fracture theories

The LEFM framework for basal-crevasses (Van der Veen, 1998) assumes an isolated basal-crevasse with a traction-free basal boundary condition. As a result, this theory does not account for the non-trivial buoyant restoring force (Yu et al., 2017; Jiménez & Duddu, 2018; Buck & Lai, 2021; Zarrinderakht et al., 2022; Coffey et al., 2023). Thus, crevasse depths derived using LEFM may be thought of as an upper bound estimate on basalcrevasse depths, and the crevasse timescales derived using LEFM (figure 3b) as lower bounds. To test the sensitivity of our results to the choice of fracture theory, we also compute crevassing timescales using the more classic zero-stress theory (Jezek, 1984; Benn et al., 2007; Nick et al., 2010; Duddu et al., 2020) and more recent horizontal force balance (HFB) theory (Buck, 2023; Coffey et al., 2023).

Under the zero-stress theory, basal-crevasses will propagate through the ice thickness until the stress of the seawater in the crack balances the background stress state in the ice at the crack tip. As such, a rift or full-thickness fracture can form from basal-crevasse propagation when the (temperature-dependent) resistive stress $R_{xx}[T(z)]$ (equation (11)) is larger than the difference between glaciostatic stress and seawater pressure, i.e. when

Zero Stress:
$$R_{xx}\left(T\left(z\right)\right) \ge p_l\left(z\right) - p_w\left(z\right),$$
 (17)

for all $0 \le \hat{z} = z/H \le 1$. Here, $p_l = \rho_i g \left(H - z \right)$ is the background glaciostatic stress and $p_w \equiv \rho_w g \left(\frac{\rho_i}{\rho_w} H - z \right)$ is the seawater pressure. The zero-stress approximation results from the assumption that there is no stress concentration at the crack tip, which corresponds physically to a situation in which many closely-spaced cracks are present (Robin, 1974; Weertman, 1974, 1977; Duddu et al., 2020). As shown in Coffey et al. (2023), this theory tends to underpredict basal-crevasse depths, relative to observations; therefore, we consider timescales derived using this theory as an upper bound on ice-shelf ice-loss timescales.

One major limitation of the zero-stress theory is that it does not satisfy a force balance in a horizontal control volume (Coffey et al., 2023). To enforce a horizontal force balance, a change in stress must occur in the unbroken ligament of ice between the surface crevasse and basal-crevasse. This change in stress results in deeper crevasses than in the zero-stress theory (Coffey et al., 2023), i.e. the resulting horizontal force balance (HFB) theory (Buck, 2023; Coffey et al., 2023) typically predicts ice to be more vulnerable to crevassing than the zero-stress theory.

Under the HFB, the rifting stress threshold has a negligible temperature dependence (Coffey et al., 2023), rendering the resulting crevasse timescale less sensitive to melt rates than in the other theories. In the limit of stably propagating, nearly intersecting, surface and basal-crevasses (Coffey et al., 2023), the unbroken ice ligament is not able to support stresses that vary with depth. As a result, the use of a force versus rheology-

dependent stress is irrelevant, and this theory is independent of ice rheology, which is beneficial because the rheology of ice is poorly constrained (Riel & Minchew, 2023; Wang et al., 2023, for example). The stress threshold under which full-thickness crevasses propagate, \overline{R}_{xx}^* , is therefore well-approximated by the isothermal result (Buck, 2023; Coffey et al., 2023),

HFB:
$$\overline{R}_{xx}^* = \frac{1}{2} \left(1 - \frac{\rho_i}{\rho_w} \right) \rho_i g H.$$
 (18)

References

597

- Adusumilli, S., Fricker, H. A., Medley, B., Padman, L., & Siegfried, M. R. (2020).

 Interannual variations in meltwater input to the southern ocean from antarctic
- ice shelves. Nat. Geosci., 13(9), 616–620. doi: 10.1038/s41561-020-0616-z
- Alley, K., Scambos, T., Miller, J., Long, D., & MacFerrin, M. (2018). Quantifying
 vulnerability of antarctic ice shelves to hydrofracture using microwave scatter-
- ing properties. Remote Sensing of Environment, 210, 297–306.
- Alley, R., Cuffey, K., Bassis, J., Alley, K., Wang, S., Parizek, B., ... DeConto, R.

 (2023). Iceberg calving: regimes and transitions. *Annual Review of Earth and*Planetary Sciences, 51(1), 189–215.
- Banwell, A. F., MacAyeal, D. R., & Sergienko, O. V. (2013). Breakup of the larsen b ice shelf triggered by chain reaction drainage of supraglacial lakes. *Geophysical Research Letters*, 40(22), 5872–5876.
- Bassis, J. N., Crawford, A., Kachuck, S. B., Benn, D. I., Walker, C., Millstein, J.,

 Luckman, A. (2024). Stability of ice shelves and ice cliffs in a changing

 climate. Annual Review of Earth and Planetary Sciences, 52.
- Bassis, J. N., Fricker, H. A., Coleman, R., & Minster, J.-B. (2008a). An investigation into the forces that drive ice-shelf rift propagation on the amery ice shelf, east antarctica. *Journal of Glaciology*, 54 (184), 17–27.
- Bassis, J. N., Fricker, H. A., Coleman, R., & Minster, J.-B. (2008b). An investigation into the forces that drive ice-shelf rift propagation on the amery ice shelf, east antarctica. *Journal of Glaciology*, 54 (184), 17–27.
- Bassis, J. N., & Ma, Y. (2015). Evolution of basal crevasses links ice shelf stability to ocean forcing. Earth and Planetary Science Letters, 409, 203–211.
- Benn, D. I., Hulton, N. R. J., & Mottram, R. H. (2007). 'Calving laws', 'sliding laws' and the stability of tidewater glaciers. Ann. Glac., 46, 123–130. doi: 10

 3189/172756407782871161
- Bett, D. T., Bradley, A. T., Williams, C. R., Holland, P. R., Arthern, R. J., & Goldberg, D. N. (2024). Coupled ice—ocean interactions during future retreat of west antarctic ice streams in the amundsen sea sector. Cryosphere, 18(6), 2653–2675. doi: 10.5194/tc-18-2653-2024
- Bradley, A. T., Bett, D. T., Dutrieux, P., De Rydt, J., & Holland, P. R. (2022). The influence of pine island ice shelf calving on basal melting. *J. Geophys. Res.*

- Oceans, 127(9), e2022JC018621. doi: 10.1029/2022JC018621
- Bradley, A. T., De Rydt, J., Bett, D. T., Dutrieux, P., & Holland, P. R. (2022).
- The ice dynamic and melting response of pine island ice shelf to calving. Ann.
- 633 Glac., 63(87-89), 111-115. doi: 10.1017/aog.2023.24
- Buck, W. R. (2023). The role of fresh water in driving ice shelf crevassing, rifting
- and calving. Earth Planet. Sci. Lett, 624, 118444. doi: 10.1016/j.epsl.2023
- .118444
- Buck, W. R., & Lai, C.-Y. (2021). Flexural control of basal crevasse opening un-
- der ice shelves. Geophys. Res. Lett., 48(8), e2021GL093110. doi: 10.1029/
- 639 2021GL093110
- Coffey, N. B., Lai, C.-Y., Wang, Y., Buck, W. R., Surawy-Stepney, T., & Hogg,
- A. E. (2023). Theoretical stability of ice shelf basal crevasses with a vertical
- temperature profile. Journal of Glaciology, 1–22.
- Coulon, V., Klose, A. K., Kittel, C., Edwards, T., Turner, F., Winkelmann, R., &
- Pattyn, F. (2024). Disentangling the drivers of future antarctic ice loss with
- a historically calibrated ice-sheet model. Cryosphere, 18(2), 653–681. doi:
- 10.5194/tc-18-653-2024
- 647 Craven, M., Allison, I., Fricker, H. A., & Warner, R. (2009). Properties of a ma-
- rine ice layer under the amery ice shelf, east antarctica. Journal of Glaciology,
- 55 (192), 717–728.
- DeConto, R. M., & Pollard, D. (2016). Contribution of antarctica to past and future
- sea-level rise. Nature, 531 (7596), 591–597. doi: 10.1038/nature17145
- DeConto, R. M., Pollard, D., Alley, R. B., Velicogna, I., Gasson, E., Gomez, N., . . .
- others (2021). The paris climate agreement and future sea-level rise from
- antarctica. Nature, 593 (7857), 83–89. doi: 10.1038/s41586-021-03427-0
- 655 Duddu, R., Jiménez, S., & Bassis, J. (2020). A non-local continuum poro-damage
- mechanics model for hydrofracturing of surface crevasses in grounded glaciers.
- J. Glaciol., 66 (257), 415–429. doi: 10.1017/jog.2020.16
- Edwards, T. L., Nowicki, S., Marzeion, B., Hock, R., Goelzer, H., Seroussi, H., . . .
- others (2021). Projected land ice contributions to twenty-first-century sea level
- rise. Nature, 593 (7857), 74–82. doi: 10.1038/s41586-021-03302-y
- Eicken, H., Oerter, H., Miller, H., Graf, W., & Kipfstuhl, J. (1994). Textural charac-
- teristics and impurity content of meteoric and marine ice in the ronne ice shelf,

- antarctica. J. Glaciol., 40(135), 386–398. doi: 10.3189/S0022143000007474
- Fisher, A. T., Mankoff, K. D., Tulaczyk, S. M., Tyler, S. W., Foley, N., & Team,
- W. S. (2015). High geothermal heat flux measured below the west antarctic ice
- sheet. Sci. Adv., 1(6), e1500093. doi: 10.1126/sciadv.1500093
- Fretwell, P., Pritchard, H. D., Vaughan, D. G., Bamber, J. L., Barrand, N. E.,
- Bell, R., ... others (2013). Bedmap2: improved ice bed, surface and thick-
- ness datasets for antarctica. Cryosphere, 7(1), 375–393. doi: 10.5194/
- tc-7-375-2013
- Fricker, H. A., Galton-Fenzi, B. K., Walker, C. C., Freer, B. I. D., Padman, L.,
- & DeConto, R. (2025). Antarctica in 2025: Drivers of deep uncertainty in
- projected ice loss. Science, 387(6734), 601–609.
- Fürst, J. J., Durand, G., Gillet-Chaulet, F., Tavard, L., Rankl, M., Braun, M., &
- Gagliardini, O. (2016). The safety band of antarctic ice shelves. Nat. Clim.
- 676 Ch., 6(5), 479–482. doi: 10.1038/nclimate2912
- Gardner, A. S., Moholdt, G., Scambos, T., Fahnstock, M., Ligtenberg, S., Van
- Den Broeke, M., & Nilsson, J. (2018). Increased west antarctic and unchanged
- east antarctic ice discharge over the last 7 years. Cryosphere, 12(2), 521–547.
- doi: 10.5194/tc-12-521-2018
- Gilbert, E., & Kittel, C. (2021). Surface melt and runoff on antarctic ice
- shelves at 1.5 c, 2 c, and 4 c of future warming. Geophys. Res. Lett., 48(8),
- e2020GL091733. doi: 10.1029/2020GL091733
- Greene, C. A., Gardner, A. S., Schlegel, N.-J., & Fraser, A. D. (2022). Antarctic
- calving loss rivals ice-shelf thinning. Nature, 609 (7929), 948–953.
- 686 Grosfeld, K., & Thyssen, F. (1994). Temperature investigation and modeling on the
- filchner-ronne ice shelf, antarctica. Ann. Glaciol., 20, 377–385. doi: 10.3189/
- 1994AoG20-1-377-385
- 689 Gudmundsson, G. (2013). Ice-shelf buttressing and the stability of marine ice sheets.
- The Cryosphere, 7(2), 647-655.
- Gudmundsson, G. H., Barnes, J. M., Goldberg, D., & Morlighem, M. (2023). Lim-
- ited impact of thwaites ice shelf on future ice loss from antarctica. *Geophys.*
- Res. Lett., 50(11), e2023GL102880. doi: 10.1029/2023GL102880
- 694 Gudmundsson, G. H., Krug, J., Durand, G., Favier, L., & Gagliardini, O. (2012).
- The stability of grounding lines on retrograde slopes. Cryosphere, 6(6), 1497—

- 696 1505. doi: 10.5194/tc-6-1497-2012
- Gudmundsson, G. H., Paolo, F. S., Adusumilli, S., & Fricker, H. A. (2019). Instan-
- taneous antarctic ice sheet mass loss driven by thinning ice shelves. *Geophys*.
- Res. Lett., 46(23), 13903-13909. doi: 10.1029/2019GL085027
- Hooke, R. L. (1981). Flow law for polycrystalline ice in glaciers: Comparison of the-
- oretical predictions, laboratory data, and field measurements. Rev. Geophys.,
- 19(4), 664-672. doi: 10.1029/RG019i004p00664
- Huth, A., Duddu, R., Smith, B., & Sergienko, O. (2023). Simulating the processes
- controlling ice-shelf rift paths using damage mechanics. Journal of Glaciology,
- 69(278), 1915-1928.
- Jezek, K. C. (1984). A modified theory of bottom crevasses used as a means for
- measuring the buttressing effect of ice shelves on inland ice sheets. J. Geophys.
- 708 Res. Solid Earth, 89 (B3), 1925-1931. doi: 10.1029/JB089iB03p01925
- Jiménez, S., & Duddu, R. (2018). On the evaluation of the stress intensity factor
- in calving models using linear elastic fracture mechanics. J. Glaciol., 64(247),
- 759–770. doi: 10.1017/jog.2018.64
- Joughin, I., & MacAyeal, D. R. (2005). Calving of large tabular icebergs from ice
- shelf rift systems. Geophysical research letters, 32(2).
- Joughin, I., Shapero, D., Smith, B., Dutrieux, P., & Barham, M. (2021). Ice-shelf re-
- treat drives recent pine island glacier speedup. Sci. Adv., 7(24), eabg3080. doi:
- 716 10.1126/sciadv.abg3080
- Kobs, S., Holland, D. M., Zagorodnov, V., Stern, A., & Tyler, S. W. (2014). Novel
- monitoring of antarctic ice shelf basal melting using a fiber-optic distributed
- temperature sensing mooring. Geophys. Res. Lett., 41(19), 6779–6786. doi:
- 720 10.1002/2014GL061155
- Lai, C.-Y., Kingslake, J., Wearing, M. G., Chen, P.-H. C., Gentine, P., Li, H.,
- ... van Wessem, J. M. (2020). Vulnerability of antarctica's ice shelves
- to meltwater-driven fracture. Nature, 584 (7822), 574–578. doi: 10.1038/
- s41586-020-2627-8
- Lhermitte, S., Sun, S., Shuman, C., Wouters, B., Pattyn, F., Wuite, J., ... Nagler,
- T. (2020). Damage accelerates ice shelf instability and mass loss in amundsen
- sea embayment. *Proc. Natl. Acad. Sci. U.S.A*, 117(40), 24735–24741. doi:
- 728 10.1073/pnas.1912890117

- Lipovsky, B. P. (2020). Ice shelf rift propagation: stability, three-dimensional effects,
- and the role of marginal weakening. The Cryosphere, 14(5), 1673–1683.
- Litwin, K. L., Zygielbaum, B. R., Polito, P. J., Sklar, L. S., & Collins, G. C. (2012).
- Influence of temperature, composition, and grain size on the tensile failure of
- vater ice: Implications for erosion on titan. Journal of Geophysical Research:
- Planets, 117(E8).
- Liu, H. W., & Miller, K. J. (1979). Fracture toughness of fresh-water ice. Journal of
- 736 Glaciology, 22(86), 135–143. doi: 10.3189/S0022143000014118
- Liu, Y., Moore, J. C., Cheng, X., Gladstone, R. M., Bassis, J. N., Liu, H., ... Hui,
- F. (2015). Ocean-driven thinning enhances iceberg calving and retreat of
- antarctic ice shelves. *Proc. Natl. Acad. Sci. U.S.A.*, 112(11), 3263–3268. doi:
- 740 10.1073/pnas.1415137112
- Luckman, A., Benn, D. I., Cottier, F., Bevan, S., Nilsen, F., & Inall, M. (2015).
- Calving rates at tidewater glaciers vary strongly with ocean temperature.
- Nature communications, 6(1), 8566.
- Luckman, A., Jansen, D., Kulessa, B., King, E., Sammonds, P., & Benn, D. (2012).
- Basal crevasses in larsen c ice shelf and implications for their global abun-
- dance. The Cryosphere, 6(1), 113–123.
- Marsh, O. J., Luckman, A. J., & Hodgson, D. A. (2024). Brief communica-
- tion: Rapid acceleration of the brunt ice shelf after calving of iceberg a-81.
- Cryosphere, 18(2), 705-710. doi: 10.5194/tc-18-705-2024
- McGrath, D., Steffen, K., Rajaram, H., Scambos, T., Abdalati, W., & Rignot, E.
- 751 (2012). Basal crevasses on the larsen c ice shelf, antarctica: Implications for
- meltwater ponding and hydrofracture. Geophysical research letters, 39(16).
- Naughten, K. A., De Rydt, J., Rosier, S. H., Jenkins, A., Holland, P. R., & Ridley,
- J. K. (2021). Two-timescale response of a large antarctic ice shelf to climate
- change. Nat. Commun., 12(1), 1991. doi: 10.1038/s41467-021-22259-0
- Nicholls, K. (1997). Predicted reduction in basal melt rates of an antarctic ice shelf
- in a warmer climate. Nature, 388(6641), 460–462. doi: 10.1038/41302
- Nick, F., Van Der Veen, C., Vieli, A., & Benn, D. (2010). A physically based calv-
- ing model applied to marine outlet glaciers and implications for the glacier
- dynamics. J. Glaciol., 56(199), 781–794. doi: 10.3189/002214310794457344
- Nye, J. F. (1955). Comments on dr. loewe's letter and notes on crevasses. J.

- Glaciol., 2(17), 512–514. doi: 10.3189/S0022143000032652
- Park, J.-Y., Schloesser, F., Timmermann, A., Choudhury, D., Lee, J.-Y., &
- Nellikkattil, A. B. (2023). Future sea-level projections with a coupled
- atmosphere-ocean-ice-sheet model. Nat. Commun., 14(1), 636. doi:
- 766 10.1038/s41467-023-36051-9
- Pettit, E., Wild, C., Alley, K., Muto, A., Truffer, M., Bevan, S., ... Benn, D. (2021).
- Collapse of thwaites eastern ice shelf by intersecting fractures. In Agu fall
- meeting abstracts (Vol. 2021, pp. C34A-07).
- Pritchard, H., Ligtenberg, S. R., Fricker, H. A., Vaughan, D. G., van den Broeke,
- M. R., & Padman, L. (2012). Antarctic ice-sheet loss driven by basal melting
- of ice shelves. *Nature*, 484 (7395), 502–505. doi: 10.1038/nature10968
- Reese, R., Gudmundsson, G. H., Levermann, A., & Winkelmann, R. (2018). The far
- reach of ice-shelf thinning in antarctica. Nat. Clim. Chang., 8(1), 53–57. doi:
- 775 10.1038/s41558-017-0020-x
- Riel, B., & Minchew, B. (2023). Variational inference of ice shelf rheology with
- physics-informed machine learning. J. Glaciol., 1–20. doi: 10.1017/jog.2023.8
- Rignot, E., Casassa, G., Gogineni, P., Krabill, W., Rivera, A., & Thomas, R.
- 779 (2004). Accelerated ice discharge from the antarctic peninsula follow-
- ing the collapse of larsen b ice shelf. Geophys. Res. Lett., 31 (18).
- doi.org/10.1029/2004gl020697
- Rignot, E., Jacobs, S., Mouginot, J., & Scheuchl, B. (2013). Ice-shelf melting around
- antarctica. Science, 341 (6143), 266–270.
- Robel, A. A., & Banwell, A. F. (2019). A speed limit on ice shelf collapse
- through hydrofracture. Geophys. Res. Lett., 46(21), 12092–12100. doi:
- 786 10.1029/2019GL084397
- Robin, G. d. Q. (1955). Ice movement and temperature distribution in glaciers and
- ice sheets. J. Glaciol., 2(18), 523-532. doi: 10.3189/002214355793702028
- Robin, G. d. Q. (1974). Depth of water-filled crevasses that are closely spaced. J.
- 790 Glaciol., 13(69), 543–543. doi: 10.3189/S0022143000023297
- Scambos, T., Fricker, H. A., Liu, C.-C., Bohlander, J., Fastook, J., Sargent, A.,
- 792 ... Wu, A.-M. (2009). Ice shelf disintegration by plate bending and hydro-
- fracture: Satellite observations and model results of the 2008 wilkins ice shelf
- break-ups. Earth and Planetary Science Letters, 280(1-4), 51-60.

- Scambos, T., Hulbe, C., & Fahnestock, M. (2013). Climate-induced ice shelf disintegration in the antarctic peninsula. *Antarctic Peninsula climate variability: His-*
- torical and paleoenvironmental perspectives, 79–92.
- Scambos, T. A., Bohlander, J., Shuman, C. A., & Skvarca, P. (2004). Glacier ac-

celeration and thinning after ice shelf collapse in the larsen b embayment,

- antarctica. Geophys. Res. Lett., 31(18). doi: 10.1029/2004GL020670
- Scambos, T. A., Hulbe, C., Fahnestock, M., & Bohlander, J. (2000). The link be-
- tween climate warming and break-up of ice shelves in the antarctic peninsula.
- Journal of Glaciology, 46(154), 516-530.
- Schmidt, B. E., Washam, P., Davis, P. E., Nicholls, K. W., Holland, D. M.,
- Lawrence, J. D., ... others (2023). Heterogeneous melting near the thwaites
- glacier grounding line. *Nature*, 614 (7948), 471–478.
- Sergienko, O., Goldberg, D., & Little, C. (2013). Alternative ice shelf equilibria de-
- termined by ocean environment. J. Geophys. Res.: Earth Surf., 118(2), 970-
- 981. doi: 10.1002/jgrf.20054

799

- Seroussi, H., Nowicki, S., Payne, A. J., Goelzer, H., Lipscomb, W. H., Abe-Ouchi,
- A., ... others (2020). Ismip6 antarctica: a multi-model ensemble of the antarc-
- tic ice sheet evolution over the 21st century. Cryosphere, 14(9), 3033–3070.
- doi: 10.5194/tc-14-3033-2020
- Seroussi, H., Verjans, V., Nowicki, S., Payne, A. J., Goelzer, H., Lipscomb, W. H.,
- ... others (2023). Insights into the vulnerability of antarctic glaciers from the
- ismip6 ice sheet model ensemble and associated uncertainty. The Cryosphere,
- 17(12), 5197-5217.
- Smith, B., Fricker, H. A., Gardner, A. S., Medley, B., Nilsson, J., Paolo, F. S.,
- ... Zwally, H. J. (2020). Pervasive ice sheet mass loss reflects compet-
- ing ocean and atmosphere processes. Science, 368(6496), 1239–1242. doi:
- 10.1126/science.aaz5845
- 822 Sun, S., Cornford, S. L., Moore, J. C., Gladstone, R., & Zhao, L. (2017). Ice shelf
- fracture parameterization in an ice sheet model. Cryosphere, 11(6), 2543–2554.
- doi: 10.5194/tc-11-2543-2017
- Sun, S., Pattyn, F., Simon, E. G., Albrecht, T., Cornford, S., Calov, R., ... others
- (2020). Antarctic ice sheet response to sudden and sustained ice-shelf collapse
- 827 (abumip). J. Glaciol., 66 (260), 891–904. doi: 10.1017/jog.2020.67

- Tada, H., Paris, P., & Irwin, G. (2000). The stress analysis of cracks handbook. The

 American Society of Mechanical Engineers.
- Tyler, S., Holland, D., Zagorodnov, V., Stern, A., Sladek, C., Kobs, S., ... Bryenton, J. (2013). Using distributed temperature sensors to monitor an antarctic ice shelf and sub-ice-shelf cavity. *J. Glaciol.*, 59 (215), 583–591. doi:
- 10.3189/2013JoG12J207
- van den Akker, T., Lipscomb, W. H., Leguy, G. R., Bernales, J., Berends, C., van de
 Berg, W. J., & van de Wal, R. S. (2024). Present-day mass loss rates are a

 precursor for west antarctic ice sheet collapse. EGUsphere, 2024, 1–25.
- Van der Veen, C. (1998). Fracture mechanics approach to penetration of bottom crevasses on glaciers. *Cold Reg. Sci. Technol.*, 27(3), 213–223. doi: 10.1016/ S0165-232X(98)00006-8
- Van der Veen, C. (2013). Fundamentals of glacier dynamics. CRC press. doi: 10

 1201/b14059
- Walker, C. C., Millstein, J. D., Miles, B. W., Cook, S., Fraser, A. D., Colliander, A.,

 ... others (2024). Multi-decadal collapse of east antarctica's conger-glenzer ice

 shelf. *Nature Geoscience*, 17(12), 1240–1248.
- Wang, Y., Lai, C.-Y., & Cowen-Breen, C. (2023). Discovering the rheology of

 antarctic ice shelves via physics-informed deep learning. doi: 10.21203/

 rs.3.rs-2135795/v1
- Wang, Y., Zhao, C., Gladstone, R., Galton-Fenzi, B., & Warner, R. (2022). Thermal structure of the amery ice shelf from borehole observations and simulations.
- Cryosphere, 16(4), 1221-1245. doi: 10.5194/tc-16-1221-2022
- Watkins, R. H., Bassis, J. N., & Thouless, M. (2021). Roughness of ice shelves is correlated with basal melt rates. Geophysical Research Letters, 48(21), e2021GL094743.
- Watkins, R. H., Bassis, J. N., Thouless, M., & Luckman, A. (2024). High basal melt rates and high strain rates lead to more fractured ice. *Journal of Geophysical Research: Earth Surface*, 129(4), e2023JF007366.
- Wearing, M. (2017). The flow dynamics and buttressing of ice shelves.
 doi: 10.17863/CAM.23327
- Weertman, J. (1974). Depth of water-filled crevasses that are closely spaced. J.

 Glaciol., 13(69), 544–544. doi: 10.3189/S0022143000023297

- Weertman, J. (1977). Penetration depth of closely spaced water-free crevasses. J. *Glaciol.*, 18(78), 37–46. doi: 10.3189/S0022143000021493
- Wilner, J. A., Morlighem, M., & Cheng, G. (2023). Evaluation of four calving laws for antarctic ice shelves. *The Cryosphere Discussions*, 2023, 1–19.
- Yu, H., Rignot, E., Morlighem, M., & Seroussi, H. (2017). Iceberg calving
 of thwaites glacier, west antarctica: full-stokes modeling combined with
- linear elastic fracture mechanics. Cryosphere, 11(3), 1283-1296. doi: 10.5194/tc-11-1283-2017
- Zarrinderakht, M., Schoof, C., & Peirce, A. (2022). The effect of hydrology and crevasse wall contact on calving. *Cryosphere*, 16(10), 4491–4512. doi: 10.5194/tc-16-4491-2022
- Zarrinderakht, M., Schoof, C., & Peirce, A. (2023). An analysis of the interaction between surface and basal crevasses in ice shelves. *EGUsphere*, 2023, 1–21. doi: 10.5194/egusphere-2023-1252

Figures

875

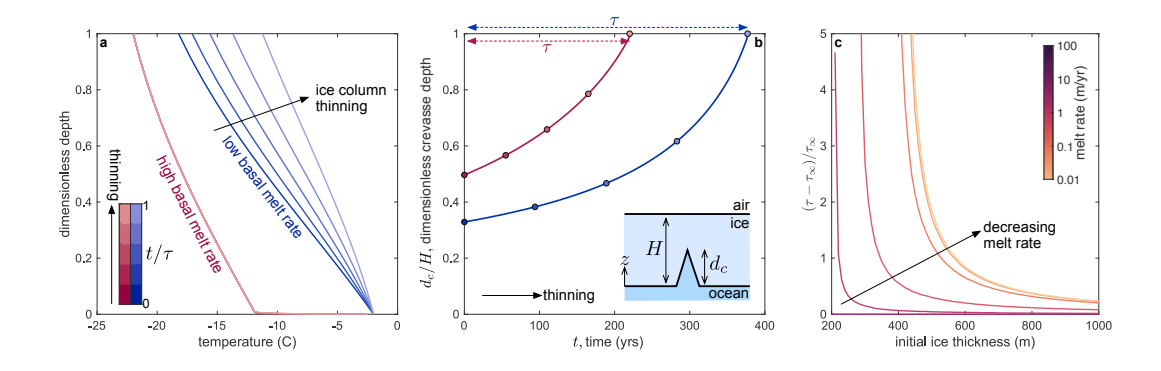


Figure 1. Basal-melt-rates strongly influence crevasse time. (a) Analytic temperature profiles (methods) for a column of ice which has a high (red hues; 48 m/yr) and low (blue hues; 0.1 m/yr) basal-melt-rate. Results are shown for different times throughout the thinning of the column of ice, as indicated by the colour bar. The quantity τ is the crevasse timescale, the time taken for the crevasse to propagate through the thickness of the ice-shelf (when $t = \tau$, a basal-crevasse has propagated through the entire thickness, see panel (b)). In both cases, the column of ice is forced to thin at a rate of 1 m/year. The high basal-melt-rate profiles are indistinguishable throughout the thinning. (b) Dimensionless crevasse depth predicted by LEFM as a function of time, throughout the thinning, for a column of ice with a high basal-melt-rate (red) and a low basal-melt-rate (blue). (c) Plot of $(\tau - \tau_{\infty})/\tau_{\infty}$, the enhancement of crevasse time, τ , over τ_{∞} , the crevasse time obtained with a very high melt rate (in this with case $\dot{m} = 250$ m year⁻¹)), as a function of initial thickness of the column. Different curves correspond to different melt rates, as indicated by the colourbar.

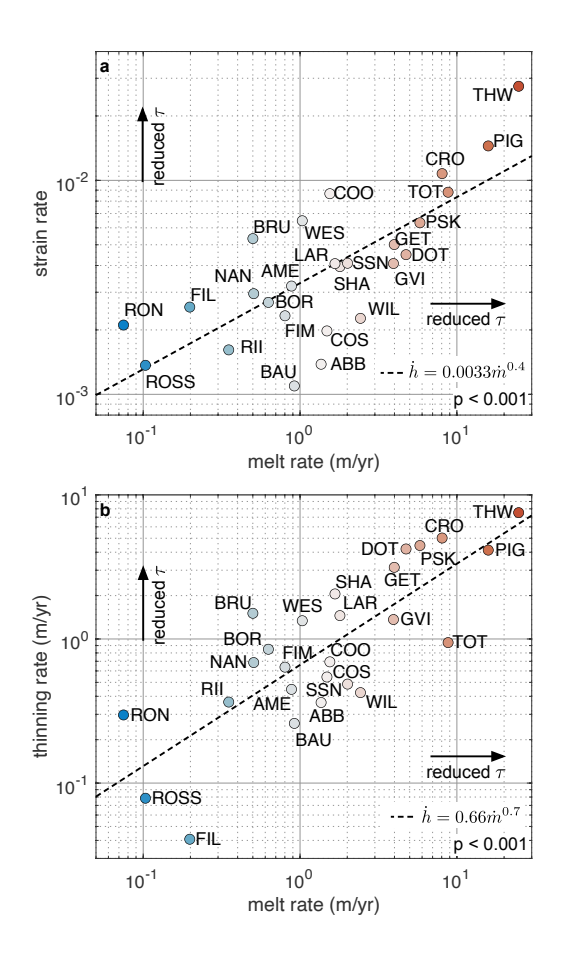


Figure 2. Thinning rate and strain rate are positively correlated with basal-meltrates on Antarctic ice-shelves. Scatter plots of ice-shelf average basal-melt-rate against (a) ice-shelf average strain rate and (b) ice-shelf average thinning rate. For each quantity, the average is determined as the arithmetic mean over all ice-shelf points. In both panels, the black dashed line indicates the best linear fit to the logarithm of the plotted quantities (for example, in (a), the dashed line is the best linear fit of log melt rates against log strain rates, see methods). In both panels, black arrows indicate the direction of reduced crevassing time τ. Here, ice-shelf names are abbreviated as follows: ABB - Abbot; AME - Amery; BAU - King Baudoin; BOR - Borchgrevink; BRU - Brunt; COS - Cosgrove; COO - Cook; CRO - Crosson; DOT - Dotson; FIL - Filchner; FIM - Fimbul and Jelbart (combined); GET - Getz; GVI - George VI; LAR - Larsen; NAN - Nansen; PIG - Pine Island; PSK - Pope, Smith and Kohler (combined); RII - Riiser Larsen, RON - Ronne; ROSS - Ross; SHA - Shackleton; SSN - Swinburne; Sulzberger and Nickersen (combined); THW - Thwaites; TOT - Totten and Moscow University (combined); WES - West; WIL - Wilkins.

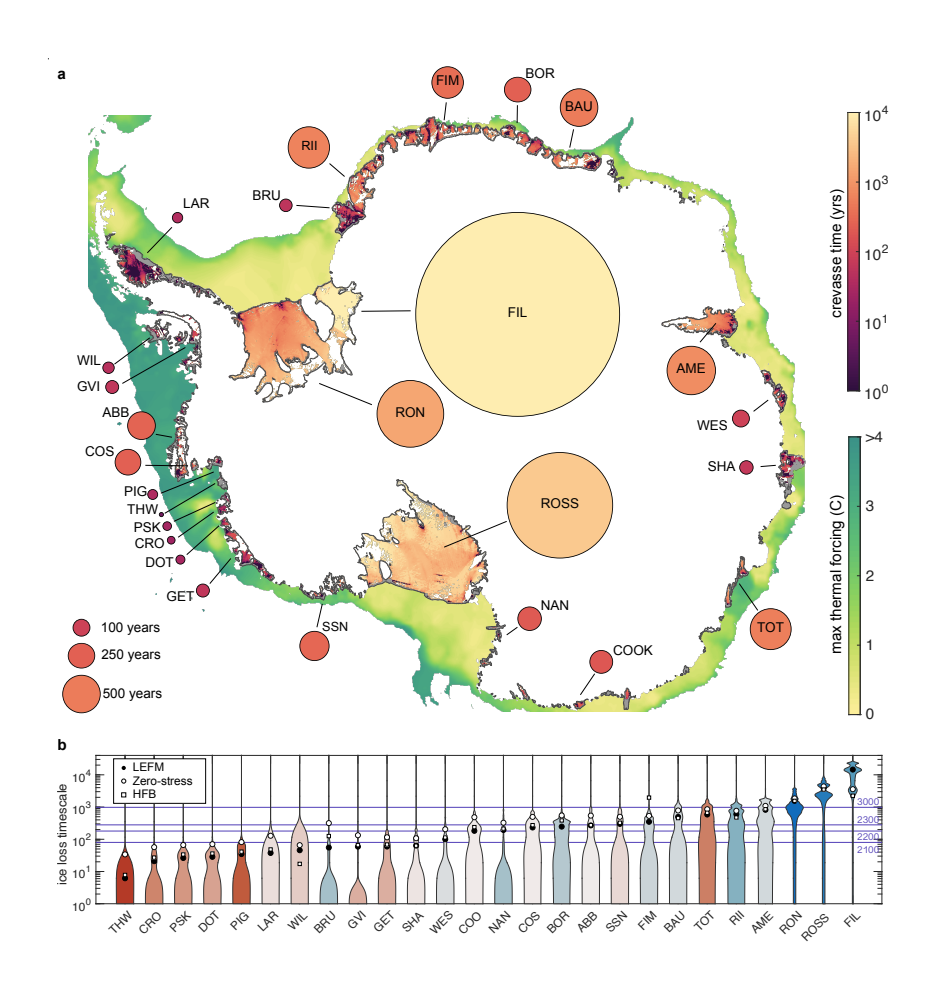


Figure 3. ice-loss timescales of Antarctic ice-shelves. (a) Circum-Antarctic crevassing timescales shown as colours in the yellow-red-black colormap. Ice-shelf locations with missing data are shown in grey. Ocean thermal forcing from ref. (Adusumilli et al., 2020) is shown in the yellow-green colormap. Filled circles show ice-loss timescales, indicated by both the area of the circle (proportional to the ice-loss timescale), and its colour (corresponds to the crevasse time colourbar). (b) Kernel density estimates of crevassing times for major Antarctic ice-shelves, shown as violin plots. For each, the black dot indicates the shelf's ice-loss timescale, computed as the mean of the kernel density estimate. White circles and square respectively indicate the ice-loss timescales obtained using the same procedure but using a crevasse depth determined by the zero-stress approximation (Nye, 1955; Jezek, 1984; Benn et al., 2007; Nick et al., 2010) and the horizontal force balance (HFB) theory (Buck, 2023; Coffey et al., 2023), rather than LEFM (methods). Shelves are ordered in order of increasing LEFM ice-loss timescale. Note that the ordinate axis in this plot is logarithmic, which gives the impression of a mean weighted towards higher crevassing times than it would otherwise with a linear ordinate axis. Background lines indicate the time to 2100, 2200, 2300 and 3000, as labelled.

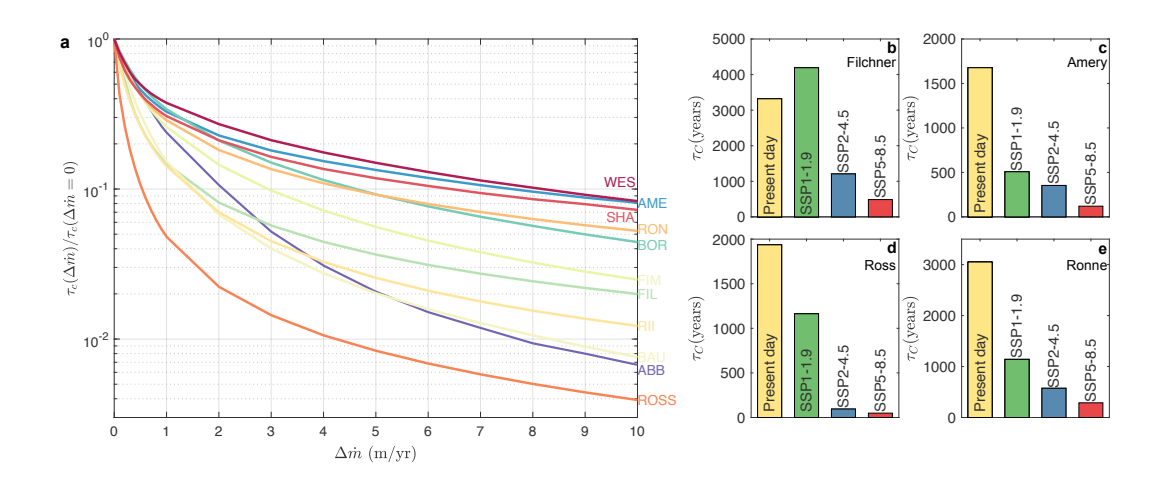


Figure 4. High sensitivity of ice-loss timescales to future increases in basal melting. (a) Semilog plot of the normalized ice-loss timescale $\tau_c(\dot{m})/\tau_c(\dot{m}=0)$, as a function of $\Delta \dot{m}$, a uniform increase in basal-melt-rate applied everywhere on the shelf. (b)–(e) ice-loss timescales of major ice-shelves under different SSP scenarios at the year 2100, with $\Delta \dot{m}$ values computed from basal-melt-rates in coupled ice-ocean-atmosphere simulations (Park et al., 2023) (methods). Each panel corresponds to a different ice-shelf, as labelled.